

Segmentations is All You Need

Zehua Cheng^{1,2,*}, Yuxiang Wu^{3,*}, Zhenghua Xu^{1,2,†}, Weiyang Wang⁴, Thomas Lukasiewicz²

¹State Key Laboratory of Reliability and Intelligence of Electrical Equipment,
Hebei University of Technology, China

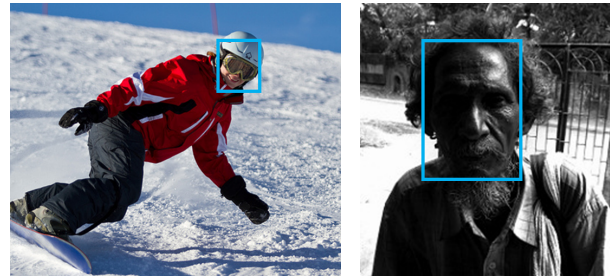
²Department of Computer Science, University of Oxford, United Kingdom

³AISA Research, Hunan Agricultural University, China

⁴SnowCloud.ai, China

Abstract

We propose a new paradigm of the detection task that is anchor-box free and NMS free. Although the current state-of-the-art model that based on region proposed method has been well-acknowledged for years, however as the basis of RPN, NMS cannot solve the problem of low recall in complicated occlusion situation. This situation is particularly critical when it faces up to complex occlusion. We proposed to use weak-supervised segmentation multimodal annotations to achieve a highly robust object detection performance without NMS. In such cases, we utilize poor annotated Bounding Box annotations to perform a robust object detection performance in the difficult circumstance. We have avoided all hyperparameters related to anchor boxes and NMS. Our proposed model has outperformed previous anchor-based one-stage and multi-stage detectors with the advantage of being much simpler. We have reached a state-of-the-art performance in both accuracies, recall rate.



(a) Occlusion Case

(b) Poor Illumination Case



(c) Large-scale Small Objects Case

Figure 1. Extreme Cases

1. Introduction

After the great success of applying deep learning to computer vision tasks [23], deep learning community has made impressive progress in various difficult tasks in the field of computer vision [18, 20], natural language processing [12, 44] and esports [45, 40].

Since detection is one of the most widely adopted tasks in real life, extreme cases always occurred. The extreme cases like complex occlusion(Figure 1(a)), poor illumination condition(Figure 1(b)), and large-scale small objects scene(Figure 1(c)) make the task more challenging. When the model encounters these extremes, the recall is unacceptably low for most widely adopted applications. To tackle this, scholars usually adopt two strategies. The first strat-

egy would train a model over a dataset with tons of extreme cases so the model could directly learn to answer the extreme cases from the data. The other strategy may base on designing a model that could tackle the extreme situation. However, designing complex models like [7] also introduce heavy engineering and highly hyperparameters-tuning required. Moreover, lead to lousy generalization when diversity growth [39]. For believers of the first strategy, more challenging datasets with well-annotated annotations and introduce well-classified difficult cases [49] have been introduced. These datasets make the evaluation of extreme cases more valuable.

The most widely adopted approaches are R-CNN approaches inherit the philosophy of regional proposal networks(RPNs) [15, 14, 33, 18]. These region proposed methods generating potential bounding boxes in an image and

*Co-first authors, contributed to this work equally.

†Corresponding author, email:zhenghua.xu@hebut.edu.cn.

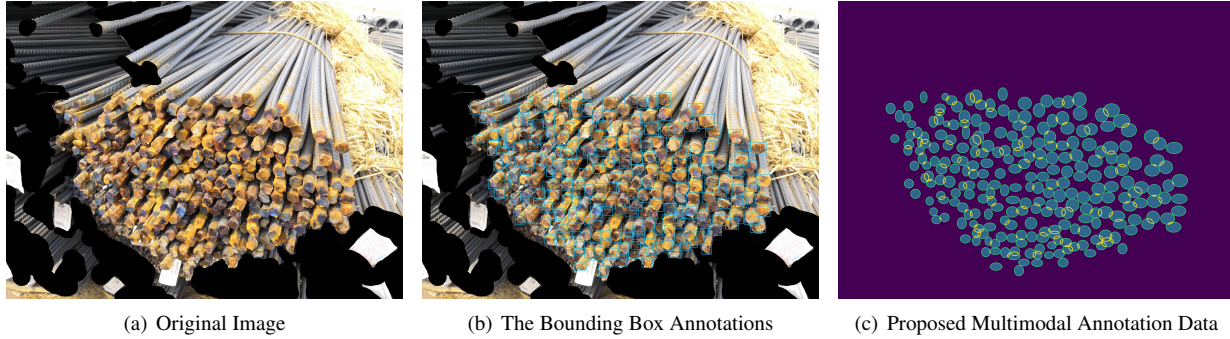


Figure 2. The traditional Bounding Box annotations(2(b)) and our proposed multimodal annotation that generated using the Bounding Box information.(2(c))

then run a classifier on these proposed Bounding Boxes. Usually, the region proposed methods can achieve high accuracy with post-processing approaches to refine the bounding boxes, eliminate duplicate detections, and restore the boxes based on other objects in the scene. However, the inherent RPN solution gets struck for the extreme cases since the Bounding Box would introduce noise which polluted the region of interest(ROI).

In extreme cases, the region proposed method encounters unsolvable bottlenecks due to NMS operations. The NMS process first ranks the scores of all the boxes and selects the highest score and the corresponding box. Then traverse the remaining boxes, delete the boxes whose IoU is greater than a certain threshold, and then continue to select the one with the highest score from the remaining boxes. Since all region proposed methods are highly required to use Non-Maximum Suppression(NMS) or its variants [4] to generate the Bounding Box. However, for complex occlusion condition, there is no appropriate threshold to achieve a good result. The successful of Cascade R-CNN [30] has also proved that variable IoU would significantly improve the performance. What's worse, the irrelevant information or the illumination and occlusion could be treated as a very tough noise which would definitely decrease the confidence. Decreased confidence also increases the difficulty of the NMS operation threshold selection. The region proposed methods highly rely on the fully supervised annotations which means the performance is related to the purity of Bounding Box [16]. And not all the people follow the existing annotating standard like [1] to build the dataset. Some of the datasets may introduce more noise during the annotating. What is worse, the Bounding Box cannot represent some challenging tasks like occlusion, small object, and illumination since the noise are introduced by the scene information. To avoid introducing noise, there is an ideal solution that introducing segmentation directly on the image. The goal of segmentation is to label each pixel of an image with a corresponding class of what is being represented. This would allow the model to perform a

pixel-level classification on the images. By introducing segmentation means the model can utilize the retrained specific topological structure of the annotations, which make occlusion problem can be alleviated by applying CNNs to learn the topological of input image [24]. The pixel-level annotation could well-describe the small objects in the scene and significantly reduce the potential of the noise introduced.

However, the cost of obtaining pixel-level segmentation masks is more than 15 times expensive than that of annotating Bounding Box on object detection task [26]. Annotating pixel-level annotations of each object class is laborious, and hampers the expansion of object classes, which have hindered the performance of CNNs that in general desire large-scale data for training. What is worse, most segmentation approaches are not instance-aware [8, 10, 11]. Transforming the segmentation result in detection without instance-aware results is hard. Even though the work finished in [8, 11] has present an instance-aware solution, but these works have introduced multiple models to process this task, which also leads to heavy engineering. To get over limitation as mentioned above, we propose to use the bounding box information to generate the segmentation-like information and use the segmentation model to perform the accurate detection with the task where the input is weak supervised Bounding Box. We propose a multimodal annotation to solve extreme cases. With multimodal annotations, the background, occlusion information could be utilized so a single segmentation model could solve the complex cases.

We have viewed that our proposed multimodal annotation method is exceptionally extendable. Any new features could easily apply for its benefits over the annotations. In our experiments, we have observed that although our results could reach a state-of-the-art performance over small objects(objects like 50×50 pixel). Some *extreme small cases* where we describe the cases as size under 15×15 pixels. These cases are usually discarded in the *small object cases* for its extreme size. However, in this work, we also introduce a novel approach using the vector field in the image. With the vector field assistance, the *extreme small cases* are

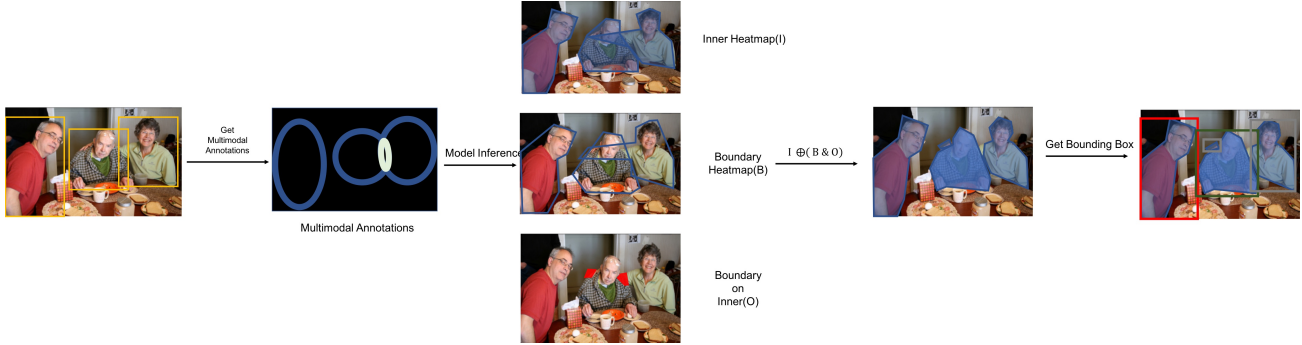


Figure 3. The process of generating our multimodal annotation in segmentation task.

conquerable.

Our multimodal annotation has an assumption that *each Bounding Box is a circumscribed quadrilateral of the geometric shape we interested*. However, in our experiments, we have observed that it is not a strict assumption, which means the given Bounding Box does not cover the object strictly, the performance still aced the state-of-the-art methods. This also indicated that even with weak-supervised segmentation annotation generated from contour tracing algorithm, our proposed method could achieve strong robustness in extreme situations including complex occlusion and extreme small object.

The contributions of this paper are as follows:

1. We proposed to use the weak reinforced inexact supervised approach to generate the segmentation map using the Bounding Box information.
2. We proposed to use multimodal annotations to achieve instance aware solution.
3. We proposed a non-NMS approach to achieve strong robustness in extreme cases.
4. We proposed to introduce vector field in our multimodal annotations to achieve state-of-the-art performance on extremely small objects.

2. Related Work

2.1. Anchor-Based Detection

Object detection task involve predicting object Bounding Boxes and categories [14, 15, 19]. The Bounding Box is an axis-aligned rectangle tightly bounding the object [13, 35] or, a precise pixel-wise segmentation mask, or a closed boundary [26, 36]. Object detection task is closely related with image segmentation which aims is to assign each pixel in an image to a semantic class label. Anchor-based detectors inherit from the traditional sliding-window and proposal based detectors. Most state-of-the-art result such as [15, 14, 33, 18] are anchor-based strategies.

Although the anchor-based solution could achieve remarkable performance, it has excessively many hyperparameters, which typically need to be tuned carefully. These hyperparameters have shown a great impact on the final accuracy, and require heuristic tuning. The region proposed methods highly rely on the fully supervised annotations which means the performance is related to the purity of Bounding Box [16]. Although [4] has presented a enhance version of NMS to solve the threshold problem to improve the detection task performance. The indeterminate NMS threshold is still turning the region proposed method unreliable, since there is no single threshold applicable for all real-world cases, hence not suitable for complicated occlusion. Meanwhile, when it comes to complex occlusion which could be regarded as the RoI has been polluted which has decreased the confidence of model extracted features. The impurities reduce the confidence of regions with high confidence, so this part of the confidence is more similar to the surrounding environment and loses the ability to distinguish effectively from unnecessary features. This phenomenon came quietly and seemed harmless to the detection task but cause a disastrous effect when it comes to processing the extremely challenging cases in Figure 1. It has a more severe impact on extreme cases. The experiments in WIDER Face dataset [49] also indicated that complex occlusion usually has low recall comparing with other situation. The occlusion information could regard as the region of interest(ROI) are profoundly affected by noise. Thus, rather than spending various efforts to ROI-based operations, it is better to solve this problem directly without using the ROI-related operations.

2.2. Bounding Box annotations for Segmentation

We denote by x the image values and y the segmentation map. The objective function of the fully supervised case is illustrated as follows:

$$J(\theta) = \log P(\mathbf{y}|\mathbf{x}; \theta) = \sum_{m=1}^M \log P(y_m|\mathbf{x}; \theta) \quad (1)$$

where the θ is the vector of DCNN parameters.

The per-pixel label distributions are computed by:

$$P(y_m|\mathbf{x};\theta) \propto \exp(f_m(y_m|\mathbf{x};\theta)) \quad (2)$$

where $f_m(y_m|\mathbf{x};\theta)$ is the output of the DCNN at pixel m .

When the image-level annotation is available, we can observe the image values \mathbf{x} and the image-level labels \mathbf{z} , but the pixel-level segmentations \mathbf{y} are latent variables. We have the following probabilistic graphical model:

$$P(\mathbf{x}, \mathbf{y}, \mathbf{z}; \theta) = \left(P(\mathbf{x}) \prod_{m=1}^M P(y_m|\mathbf{x};\theta) \right) P(\mathbf{z}|\mathbf{y}) \quad (3)$$

[9] has proposed to get the segmentation map from the well-annotated Bounding Box annotations where automatically generating region proposals and training convolutional networks recursively. However, since [9] is an RPN approach, the performance of this work in complex occlusion and small object is highly weak-kneed with low recall. The objective function is to maximize the IoU of Bounding Box and segmentation mask.

$$\mathcal{E}_r = \sum_p e(X_\theta(p), l_S(p)) \quad (4)$$

Here l_S is the estimated semantic label used as supervision for the network training. This objective function is the same as [31] proposes an expectation-maximization algorithm with a bias to enable the network to estimate the foreground regions. We compare with these works in the result sections.

2.3. Instance Aware Segmentation

The conventional FCNs do not work for the instance-aware semantic segmentation task, which requires the detection and segmentation of individual object instances. The inherent limitation is caused by the translation invariant of the convolution operation, which means that the corresponding image pixel receives the equivalent responses (thus classification scores) irrespective to its relative position in the context. Although the segmentation task generates the pixel-level segmentation map, the leading methods are unable to identify object instances. The instance aware segmentation share a similar structure: two subnetworks are used for object segmentation and detection sub-tasks, separately and sequentially [8, 10, 11, 17]. They can be easily made for convenience other than for fundamental considerations.

3. Methodology

3.1. Model Structure

In this section, we first reformulate object detection in a pixel-level annotation mask. Besides that, the inner and outer information would also bring better representation to the pixel-level annotations. Since the inner, outer and boundary information has been highlighted by the introduced additional information. It would help the FCN-based model like UNet [34] to extract more details that are beyond the topological form. This would also be eliminating the side effects of the high original resolution which unavoidably sacrifice the purity of the region of the interest(RoI). Therefore, we combine internal, external and boundary information with pixel-level annotation into the multimodal annotation. Our proposed structure is presented in Figure 3. The system takes a color image of size (*height, width, channel*) as input to produce a sequence of x, y coordinates of boundary pixels as output. When training phase, our CNN target multimodal annotation heatmaps(Figure 2(c)), which are produced by the given Bounding Box. When inferencing phase, our find contour algorithm parses multimodal results to output the localization of all objects. To further illustrate our proposed method, we discuss the details of the multimodal annotations in Section 3.2, the details of the *Contour Tracing* that presented in the Figure 3 is lies in Section 3.4. The Section 3.3 illustrate the details of the training process.

3.2. Multimodal Annotations

The motivation of our multimodal annotations strategy came from a simple fact that segmentation usually has better representation and have a strong ability to solve some tough cases that the detection cannot solve. However, the pixel-level segmentation mask does not fully utilize by the models [9]. The generated mask is not really pixel-level since the models that with strong details have the potential to over-fitting, which definitely not are regarded, successful models. We have taken into serious consideration about the fact that claimed at the beginning of this paragraph. Therefore, we draw a conclusion that the well-designed pixel-level segmentation mask may not essential. The rest of the elements of the segmentation mask are *pixel-level annotation* and *geometric shape*. We viewed the pixel-level is an essential representation method for utilizing the geometric shape. In such cases, we simplify the essential elements of a **strong representation annotations** as **simple geometric pixel-level annotations**. With the existing information for the detection task, we turned our attention to transform the bounding box(BBox) to generate weak-supervised segmentation map with a pixel-level simple geometric shape.

Since the inexact supervision which usually causes a disaster in occlusion and small object condition [52], we

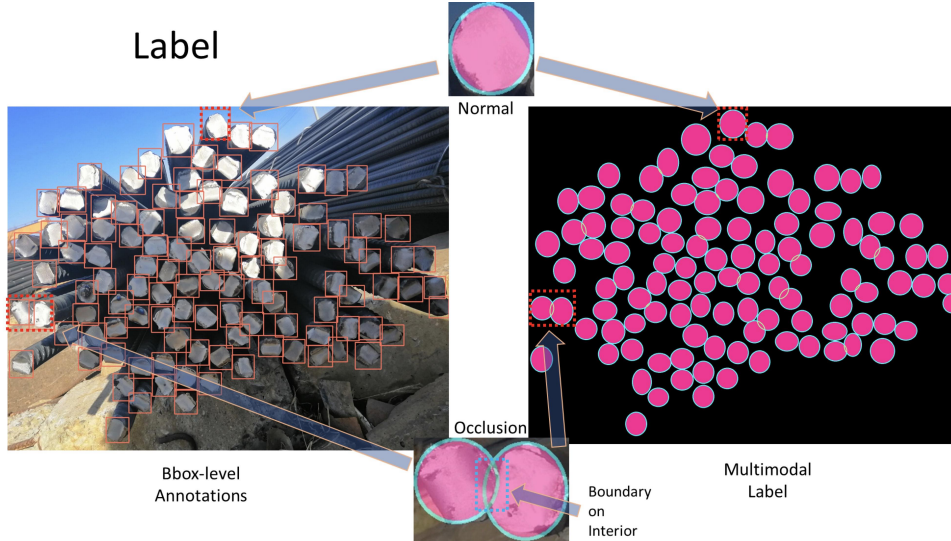


Figure 4. Details of our proposed multimodal annotations.

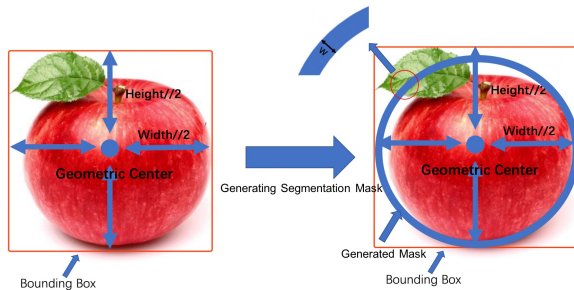


Figure 5. The First Step of transforming the bounding box annotation to the multimodal annotations.

have to solve the unsatisfying performance by introducing additional information to the annotations. This approach helps this method to have stronger representation and also achieve better performance on detection. We assume that each Bounding Box is a circumscribed quadrilateral of the geometric shape of the corresponding object. The boundary is defined as a complete contour line, which is defined as a segment of one or more pixels in width and length and is used to describe the shape of the object and its relationship with other objects. The detected contours are reinforced in exact supervision. In Figure 5, we have present an example of transforming the *box-level* annotations to *pixel-level* annotations. The generated pixel-level annotations allow fully supervised segmentation to achieve reliability in learning the boundaries of objects and the relationship between their components. In given information of the Bounding Box including the width and height of the bounding box shape and the geometric center of the object. By transforming the objects, we would get an easy geometric shape of the objects. In such a case, the annotation would become a hollow shape

with a *width* = w . This process is described in details in the Algorithm 1. However, roughly applying the contour information to generate the segmentation map would be lost the semantic information since the Bounding Box has a clear boundary while merging the pixel-level annotations would break the boundary of the information. So we proposed a novel strategy to generate the information of bilateral occlusion relationship. For given the object A and object B , we have got three conditions:

- A blocked B .
- B blocked A .
- Non-occlusion relationship between A and B (no intersection).

As Figure 4 presented, we denoted the annotations as follows:

- Background.
- Ordinary Interior Section.
- Ordinary Boundary.

The Figure 2(c) has presented our multimodal annotations that generated from the Bounding Box information in Figure 2(b). We combine these three conditions as additional annotations with our proposed approach to train the model.

3.3. Training Process

The process is presented in Figure 3. We discuss the details of our training process in this section. We have adopted a novel structure to make full use of the details in the segmentation tasks with Hourglass model. The model structure is presented in Figure 6 and Figure 7, the first stage would produce a set of abstract feature $S^1 = h(I)$, where h are the head of our model. Moreover, in each subsequent stage, the

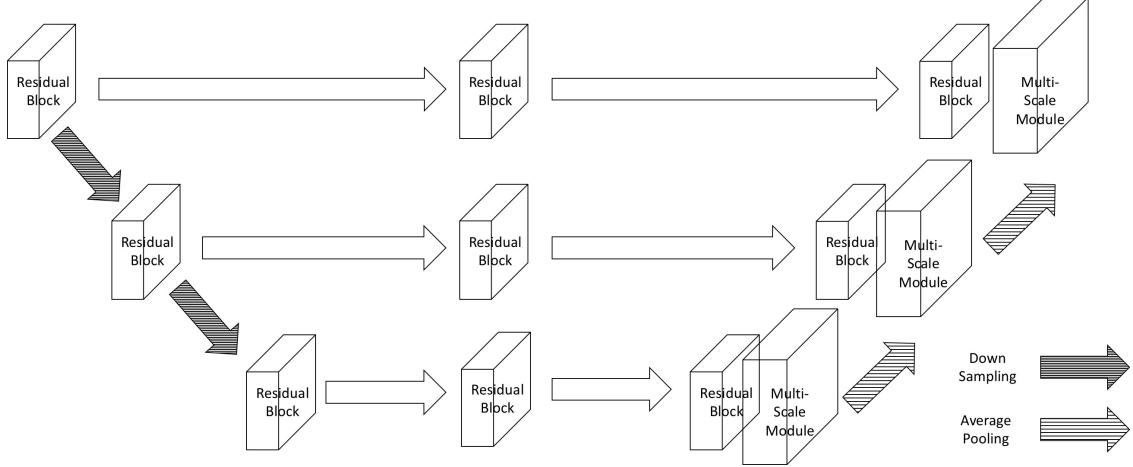


Figure 6. Proposed MultiScale Model Structure

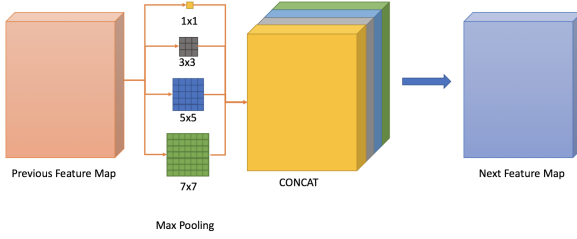


Figure 7. MultiScale Block

block inherits multiscale information in the previous stage to produce more robust features $S^t = Fox(S^{t-1})$. At the end, two different point-wise convolution generate segmentation result $C = d_1(S^t)$ and feature result $F = d_n(S^t)$, where d is the depth-wise convolution and n is the number of channel of them. In order to fully utilize the facial multi-scale information, we proposed to use Hourglass [28], as our backbone. Noted that the stacked Hourglass backbone. We also perform the ablation study in Table 1 and Table 2.

The loss function of our proposed model is defined as follows:

$$L_{var} = \frac{1}{C} \sum_{c=1}^C \frac{1}{N_c} \sum_{i=1}^{N_c} [\cosine(\mu_c, x_i) - \delta_v]_+^2 \quad (5)$$

$$L_{dist} = \frac{1}{C(C-1)} \sum_{c_A=1}^C \sum_{c_B=1}^C \frac{1}{N_c} \sum_{i=1}^{N_c} [2\delta_d - \cosine(\mu_{c_A}, \mu_{c_B})]_+^2 \quad (6)$$

$$L_{reg} = \frac{1}{C} \sum_{c=1}^C (\|\mu_c\|_2 - R)^2 \quad (7)$$

$$L_{fox} = \alpha \cdot L_{var} + \beta \cdot L_{dist} + \gamma \cdot L_{reg} \quad (8)$$

The variance term (L_{var}) is an intra-cluster pull-force that draws embeddings towards the mean embedding which

has presented in Equation 5. The distance term is an inter-cluster push-force that pushes clusters away from each other, increasing the distance between the cluster centers which has presented in Equation 6. The regularization term is a small pull-force that draws all clusters towards the origin, to keep the activations bounded which has presented in Equation 7. In the equations, the definitions are as follows: C is the number of clusters in the ground truth, N_c is the number of elements in cluster c , x_i is an embedding, μ_c is the mean embedding of cluster c (the cluster center), $\cosine(a, b)$ is the cosine loss between a and b , which could also be noted as $\frac{a \cdot b}{\|a\| \cdot \|b\|}$. $[x]_+ = \max(0, x)$ denotes the hinge. δ_v and δ_d are respectively the margins for the variance and distance loss.

We put the bounding box level annotations and the original image as the input. The first process would be transforming the bounding box to the multimodal annotations. We only use the generated multimodal annotations as our training target. Since the segmentation results are always coarse, our segmentation results do not have an adorable shape even the original input information is made up of simple geometry with occlusion information as stated above. Meanwhile, the output results are also numerical and our goal is not to perform segmentation on the image but to get a good performance on detection. Therefore, we transform the numerical segmentation results in binary results.

We use binary cross-entropy as our loss function (Equation 9).

$$H_p(q) = -\frac{1}{N} \sum_{i=1}^N y_i \cdot \log(p(y_i)) + (1 - y_i) \cdot \log(1 - p(y_i)) \quad (9)$$

Where y is the label, $p(y)$ is the prediction probability of all N samples. This result would be a binary image, in which case the foreground is 1 and the background is 0.

We developed a contour tracing algorithm(see the details in Section 3.4) to detect the edges of a given region in the Bounding Box to generate the simple geometric shape as presented in Figure 3.3. With the generated contour information, we could generate the segmentation map inside the Bounding Box.

Algorithm 1 Transferring Bounding Box Annotations to Multimodal Annotations

Input: $\mathcal{B} = \{b_1, \dots, b_N\}, \mathcal{S} = \{s_1, \dots, s_N\}, N_t$

- 1: \mathcal{B} is the list of Bounding Boxes.
- 2: \mathcal{W} is the width of contour.

Output: label heatmap of interior, contour, contour on interior

- 3: **for** b in \mathcal{B} **do**
- 4: $x, y, width, height \leftarrow b$
- 5: Center point of inscribed ellipse P_c of $b \leftarrow (width//2, height//2)$
- 6: Interior ellipse \leftarrow a solid ellipse whose axes are $width//2 - w$ and $height//2 - w$
- 7: Interior mask \leftarrow a matrix of interior ellipse, other pixels are 0
- 8: Object ellipse \leftarrow a hollow ellipse whose axes are $width//2$ and $height//2$
- 9: Contour mask \leftarrow a matrix of interior ellipse *XOR* object ellipse, others are 0
- 10: Interior Heatmap $[x : x + weight, y : y + height] \leftarrow$ Interior mask
- 11: Contour Heatmap $[x : x + weight, y : y + height] \leftarrow$ Contour mask
- 12: **end for**
- 13: Contour on Interior Heatmap \leftarrow Interior heatmap intersect contour heatmap

3.4. Object Localization by Contour Tracing Algorithm

The main problem is how to localize all the existing objects. We utilize Contour Tracing algorithm to take the multimodal heatmaps that generated by our deep learning models(i.e. UNet [34]), which is the Interior Heatmap(I), the Boundary Heatmap(B) and the Boundary on Interior(O). To producing cartesian coordinates of boundaries of all objects. We adapt our strategy as follows:

1. Pruning the interior heatmap and generating binary images [41].
2. Parsing the coordinates of boundaries from the binary image.

Generating Binary Image Limited by network training degree, when an object is closer to other objects, the interior of the object becomes viscous with others and the region goes larger including others, so that the detection of

object boundaries has an irreversible effect. So we design a method to prune the viscous pixels utilizing our multimodal heatmaps.

As shown below:

$$I \oplus (B \& O) \tag{10}$$

Before tracing contour, the 8-bit heatmaps need to transfer to binary image [41]. So we threshold the pruned image and obtain a binary image which foreground is 1, background 0.

Run-data-based Following Algorithm

One conventional way to trace contour is using scan-based-following algorithm after image binarization, pixel by pixel connected into contour[41]. However, in the case of a large image with many objects, the most situation we are, time consumption will be quite high[37]. The reason is that this algorithm will raster scan the whole image to find the starting point first and trace edge point one by one, and resume the scan from the next pixel to find the next starting point.

For less time and memory consuming, we propose a modified run-data-based(RDB) following algorithm that uses only one or two line buffers and loads all pixel only once[2]. So we use RDB following algorithm to trace our rebar dataset which has a host of rebar head in an image and output a sequence of coordinates of pixels of object boundaries. We view the minimum and maximum x and y value as the top-left and bottom-right coordinates of Bounding Box.

Algorithm 2 Run-data-based following algorithm

Input: A binary image with h (height) and s (width).

- 1: $l_{edge} \leftarrow$ the pixel (j, i) whose value is 1 and left pixel is 0.
- 2: $r_{edge} \leftarrow$ the pixel (j, i) whose value is 1 and right pixel is 0.
- 3:

Output: A list of contour pairs sets.

- 4: **for** j in h **do**
- 5: **while** Scan the j row **do**
- 6: Find a pair m of l_{edge}^j and r_{edge}^j
- 7: **if** $\left| X_{l_{edge}}^j(m) - X_{l_{edge}}^{j-1}(n) \right| \leq 1$ and $\left| X_{r_{edge}}^j(m) - X_{r_{edge}}^{j-1}(n) \right| \leq 1$ **then**
- 8: Add the pair to the contour set of the pair n
- 9: **else**
- 10: Create a new contour set with this pair
- 11: **end if**
- 12: **end while**
- 13: **end for**

3.5. Vector Field in Training Extreme Small Cases

During our training process, we have found that even with our strategy, it is still hard for the model to learn the

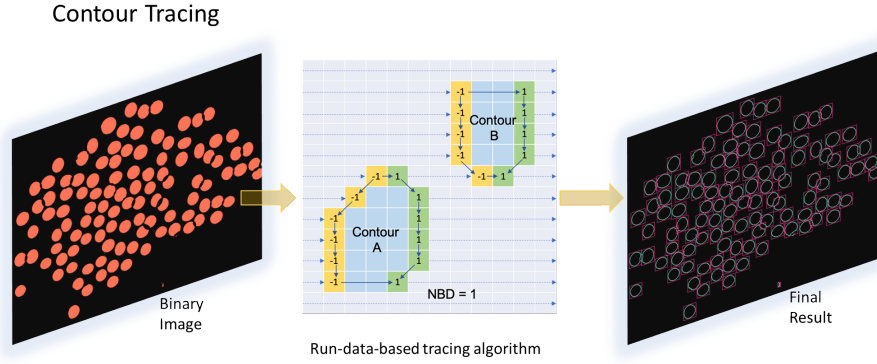


Figure 8. Contour Tracing Algorithm

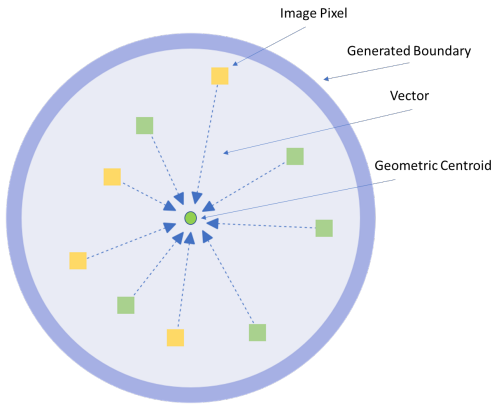


Figure 9. The process of introducing the vector field in extreme small cases in the scene.

features of the extreme small cases (like the objects only place in several pixels), it is possible for the model to learn the prior information in the scene.

In order to prevent these cases, we are introducing a vector field in our multimodal annotation. The details of this method are displayed in Figure 9. The vector field is extracted by assigning every image pixel within the detected boundary to a vector pointing to the geometric centroid. In Figure 9, the whole area (both the background and the boundary) is a multimodal annotation generated in Figure 4. We left out the occlusion information inside the annotation and described the typical scene in Figure 9. Each of the image pixel within the area is the start point where has been present as a little square in Figure 9 and has assigned its direction to the geometric centroid. The vector field in Figure 9 is an arrow pointing from a square (image pixel) to the center of the geometry.

4. Experiment

To show the strength of our proposed NMS and anchor-box free paradigm, we have tested our model on Rebar Head Detection Challenge Dataset¹, WiderFace Dataset² and MS COCO Detection Dataset³. We adopt Hourglass [28] to perform the ablation study. In Table 1 and Table 2, the *Stack* is the number of stacked hourglass networks. *Base* represents the base of a convoluted channel, such as the initial convolution kernel of the Hourglass is 7×7 with input 256 or $4 \times base$ so the *Base* is 64. *Depth* denotes the number of downsampling in Hourglass. The stem represents the three consecutive 3×3 convolution with the strides of 1 before the first stack. In order to get more local features of scale in the decoder, we use average pooling of three scales (1, 3, 5) to obtain multi-scale sensory fields. Since the kernel size = 1 does not require additional processing, we denote it as *avg(3,5)*. The *#params* refers to the number of parameters for the corresponding networks. All models are implemented using PyTorch [32], and trained on a GPU server with 8 NVIDIA GTX 1080Ti GPU. Some important training details are as follows: (i) the batch size is 8/GPU. (ii) the all models are learned using the sgd optimizer with warm up [27] with 3 warm-up epochs, the momentum = 0.9. The additional details of the experiments are presented in each table. (iii) We use the cosine decay [48] strategy.

We adopt the multimodal annotation strategy to generate the interior and boundary of the object according to the Bounding Box by Section 3.2.

4.1. Rebar Head Detection

Rebar Head Detection Dataset possesses 250 train images (including 30942 rebar heads) and 200 test images. The original resolution of the whole image is 2000×2666 . The objective rebar head is really small. The average area of

¹<https://www.datafountain.cn/competitions/332/details>

²<http://mmlab.ie.cuhk.edu.hk/projects/WIDERFace/>

³<http://cocodataset.org/>

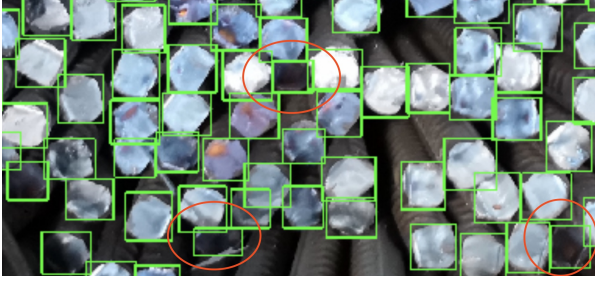


Figure 10. An Example of Complex Occlusion in Rebar Head Detection Dataset

each box is 7,000 pixels, accounting for 0.13% of the whole image. It is a relative small dataset(only 250 training samples) but there are many objects in single image. The image is poor annotated and rich in diverse illuminations and serious occlusions(see Figure 10, the red circle has presented the occlusion condition of the target image).

Experiment Result We select Faster R-CNN [33] and Cascade R-CNN [6] as our baseline since these are the most popular anchor-based model with very good performance. The Table 1 has presented the results of the Rebar Head Detection Dataset. Because the input resolution is 2000×2666 which is too big for the model to learn the details.

In the Table 1, our proposed method with $Stack = 2$, $Base = 40$, $Depth = 5$ has reached the best performance in Rebar Head Dataset Challenge. However, considering the Cascade R-CNN is a multi-stage strategy that performs the cascade regression strategy to increase the IoU value of proposals step by step with a resampling mechanism. Such operations resulted in huge model sizes. In Table 1, the params size of the Cascade RCNN has reached to the 42.1M, which is 7 times then our proposed method.

4.2. WIDER Face Detection Dataset

WIDER Face Detection Dataset [49] owns 32,203 images and 393,703 faces. Faces in the proposed dataset are extremely challenging due to high degree of variability in scale, pose and occlusion. WIDER Face has much lower detection rate compared with other face detection datasets. WIDER Face has three levels of difficulty defined by *Easy*, *Medium*, *Hard* based on the detection rate of EdgeBox [54]. What’s more, the dataset also treat occlusion as an additional attribute and assign the datasets into three categories: *no occlusion*, *partial occlusion*, and *heavy occlusion*. A face is annotated as *partial occlusion* when there is 1% to 30% of the total face area is occluded. A face with the occluded area over 30% is labeled as *heavy occlusion*. We have set 12879 for the training set, 3226 for the validation set, and 16098 for the test set. The details of the attributes of the dataset are presented as follows:

Experiment Result We select the most representative baseline in [49] i.e. Two-stage CNN, Cascade R-CNN,

and the state-of-the-art model like LDCF+[29], multitask Cascade CNN [51], ScaleFace [50], MSCNN [5], HR [21], Face R-CNN [47], Face Attention Networks [46] and PyramidBox [43] as our baseline⁴. Some of the models are the most popular model in the area while some of the models have reached state-of-the-art performance in this task.

The experiment results are presented in Table 11 and Table 2. Although the WiderFace dataset has provided an Precision-Recall(PR) curve which presenting different thresholds to get the different recall-precision pairs of different models. However, as a new paradigm, our approach has presented a 100% confidence ratio. That is, to find out is to confirm 100% that the set of pixels is the edge of an object, so the score is always 1. Hence, the metric is not suitable to measure the robustness of our proposed paradigm. So we compare our unique recall-precision F1 score with the maximum F1 score of other detection methods. The results in Figure 11 has been proved that our F1 scores in *easy*, *medium* and *hard* have aced the state-of-the-art models which is **94.70**, **93.41**, **87.23** respectively.

To further analysis the model, we perform an ablation study on WIDER Face dataset in Table 2.

4.3. MS COCO Detection Dataset

MS COCO Detection Dataset [26] is one of the most popular large-scale detection task. We test our paradigm in MS COCO dataset. We use the COCO trainval135k [3] split(115K images) for train and minival split(5K images) as validation. The results of the MS-COCO is presented in Table 3. We report our main results on the test-dev split(20k images) with a host of the detection method. We have set 82081 for the training set, 40137 for the validation set, and 20288 for the test set.

We use the proposed metrics in the [26] to characterizing the performance. The metrics are noted as follows:

- **Average Precision (AP):**

- AP^s : AP for small objects: $area < 32^2$
- AP^m : AP for medium objects: $32^2 < area < 96^2$
- AP^l : AP for large objects: $area > 96^2$

- **Average Recall (AR):**

- AR^1 : AR given 1 detection per image
- AR^{10} : AR given 10 detections per image
- AR^{100} : AR given 100 detections per image

- **AR Across Scales:**

- AR^s : AR for small objects: $area < 32^2$

⁴Some code hasn’t released in public, and some of the works that we adopted using PyTorch does not reach the same performance as the paper has presented.

Method Backbone	Stack	Base	Depth	#parms	Epoch	F1 Score
Faster RCNN	-	-	-	23.2M	100	98.30%
Cascade RCNN [6]	-	-	-	42.1M	100	98.70%
Ours	1	72	3	6.1M	70	94.27%
Ours	2	40	5	5.8M	70	98.83%
Ours	4	28	5	5.7M	70	96.26%

Table 1. Ours method versus standard object detection method on Rebar Head Dataset

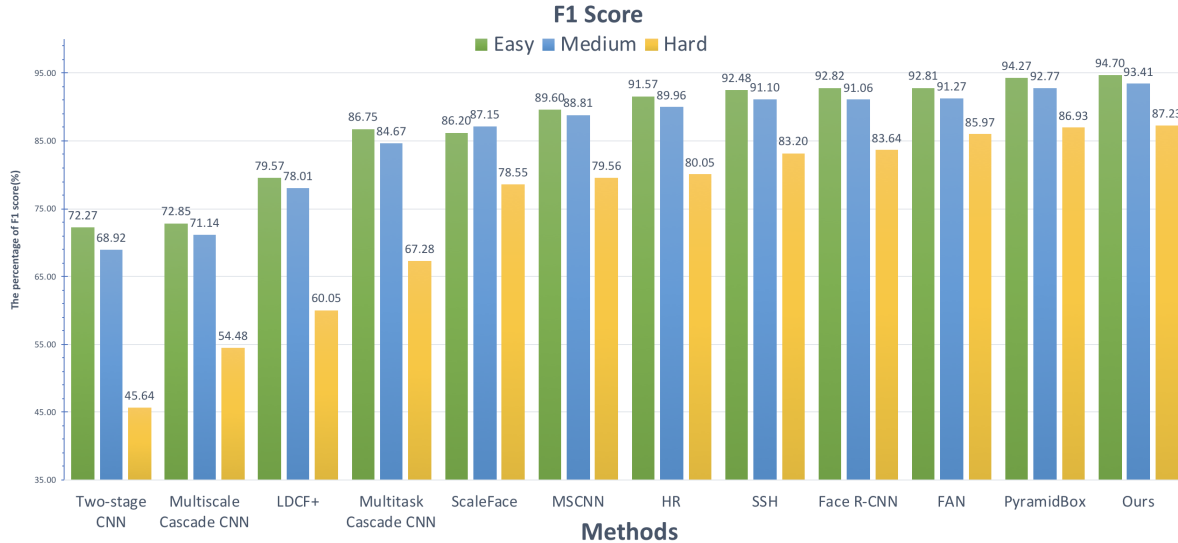


Figure 11. F1 Scores on WiderFace Val Dataset

- AR^m : AR for medium objects: $32^2 < \text{area} < 96^2$
- AR^l : AR for large objects: $\text{area} > 96^2$

Experiment Result In Table 3, the AP score of our proposed is close to that of the state-of-the-art model under different conditions. Meanwhile, our average recall rate has been significantly improved. We have viewed that the Cascade R-CNN [6] has reached the best precision in the COCO detection task. However, our proposed method is very close to the best performance. While in the Average Recall(AR) section. We have viewed that our proposed method has aced all state-of-the-art methods. For the Average Recall Across Scales metrics, we are significantly better than all the state-of-the-art models. The AR^1 of our proposed method is 35.2%, our proposed method is 6.9% higher than the second place method. The AR^s of our proposed method is 36.1%, our proposed method is 15.4% higher than the second place method.

5. Conclusion

References

[1] Voc2011 annotation guidelines. [http://host.robots.ox.ac.uk:8080/pascal/VOC/voc2012/](http://host.robots.ox.ac.uk:8080/pascal/VOC/voc2012/guidelines.html)

[guidelines.html](http://host.robots.ox.ac.uk:8080/pascal/VOC/voc2012/guidelines.html), 2012.

[2] A. K. Agrawala and A. V. Kulkarni. A sequential approach to the extraction of shape features. *Computer Graphics and Image Processing*, 6(6):538–557, 1977.

[3] S. Bell, C. Lawrence Zitnick, K. Bala, and R. Girshick. Inside-outside net: Detecting objects in context with skip pooling and recurrent neural networks. In *Proceedings of the IEEE conference on computer vision and pattern recognition*, pages 2874–2883, 2016.

[4] N. Bodla, B. Singh, R. Chellappa, and L. S. Davis. Softnms—improving object detection with one line of code. In *Proceedings of the IEEE International Conference on Computer Vision*, pages 5561–5569, 2017.

[5] Z. Cai, Q. Fan, R. S. Feris, and N. Vasconcelos. A unified multi-scale deep convolutional neural network for fast object detection. In *European conference on computer vision*, pages 354–370. Springer, 2016.

[6] Z. Cai and N. Vasconcelos. Cascade r-cnn: Delving into high quality object detection. In *Proceedings of the IEEE Conference on Computer Vision and Pattern Recognition*, pages 6154–6162, 2018.

[7] C. Chi, S. Zhang, J. Xing, Z. Lei, S. Z. Li, and X. Zou. Selective refinement network for high performance face detection. *arXiv preprint arXiv:1809.02693*, 2018.

[8] J. Dai, K. He, Y. Li, S. Ren, and J. Sun. Instance-sensitive fully convolutional networks. In *European Conference on*

Exp.	Stem	PP Block	Stack	Base	Depth	#params	Time	Epoch	Easy	Medium	Hard
1	✓	$avg(3, 5)$	2	40	5	6.08	32.19	65	94.7%	93.41%	87.23%
2		$avg(3, 5)$	2	40	5	5.78	29.47	65	91.45%	90.50%	82.86%
3	✓	$avg(3, 5)$	2	40	5	6.07	32.16	65	93.83%	92.56%	84.33%
4	✓		2	40	5	5.55	30.52	65	89.57%	88.85%	79.56%
5	✓	$avg(3, 5)$	4	28	5	5.68	34.58	65	90.53%	90.01%	82.54%
6	✓	$avg(3, 5)$	1	72	3	6.13	32.17	65	90.67%	89.86%	82.31%

Table 2. Ablation study on Widerface Val Dataset

Method	Backbone	AP^s	AP^m	AP^l	AR^1	AR^{10}	AR^{100}	AR^s	AR^m	AR^l
CoupleNet [53]	ResNet-101	13.4	38.1	50.8	30.0	45.0	46.4	20.7	53.1	68.5
Faster R-CNN	ResNet-101-C4	15.6	38.7	50.9	-	-	-	-	-	-
Faster R-CNN	ResNet-101-FPN [25]	18.2	39.0	48.2	20.0	29.3	29.7	7.2	34.8	44.4
Faster R-CNN	VGG-16 [38]	7.7	26.4	37.1	23.8	34.0	34.6	12.0	38.5	54.4
Faster R-CNN by G-RMI [22]	Inception-ResNet-v2 [42]	13.5	38.1	52.0	-	-	-	-	-	-
Mask R-CNN	ResNeXt-101	22.1	43.2	51.2	21.6	30.2	30.6	11.2	34.6	42.2
Cascade R-CNN [6]	ResNet-101	23.7	45.5	55.2	-	-	-	-	-	-
DSOD300	DS/64-192-48-1	9.4	31.5	47.0	27.3	40.7	43.0	16.7	47.1	65.0
SSD513	Resnet-101	10.2	34.5	49.8	28.3	42.1	44.4	17.6	49.2	65.8
Ours	FOXNet	22.5	41.0	51.9	35.2	52.1	57.8	36.1	58.4	73.2

Table 3. Our method versus standard object detection method on MS COCO *test - dev*

- Computer Vision*, pages 534–549. Springer, 2016.
- [9] J. Dai, K. He, and J. Sun. Boxesup: Exploiting bounding boxes to supervise convolutional networks for semantic segmentation. In *Proceedings of the IEEE International Conference on Computer Vision*, pages 1635–1643, 2015.
- [10] J. Dai, K. He, and J. Sun. Convolutional feature masking for joint object and stuff segmentation. In *Proceedings of the IEEE Conference on Computer Vision and Pattern Recognition*, pages 3992–4000, 2015.
- [11] J. Dai, K. He, and J. Sun. Instance-aware semantic segmentation via multi-task network cascades. In *Proceedings of the IEEE Conference on Computer Vision and Pattern Recognition*, pages 3150–3158, 2016.
- [12] J. Devlin, M.-W. Chang, K. Lee, and K. Toutanova. Bert: Pre-training of deep bidirectional transformers for language understanding. *arXiv preprint arXiv:1810.04805*, 2018.
- [13] M. Everingham, L. Van Gool, C. K. Williams, J. Winn, and A. Zisserman. The pascal visual object classes (voc) challenge. *International journal of computer vision*, 88(2):303–338, 2010.
- [14] R. Girshick. Fast r-cnn. In *Proceedings of the IEEE international conference on computer vision*, pages 1440–1448, 2015.
- [15] R. Girshick, J. Donahue, T. Darrell, and J. Malik. Rich feature hierarchies for accurate object detection and semantic segmentation. In *Proceedings of the IEEE conference on computer vision and pattern recognition*, pages 580–587, 2014.
- [16] Y. Guo, Y. Liu, A. Oerlemans, S. Lao, S. Wu, and M. S. Lew. Deep learning for visual understanding: A review. *Neuro-computing*, 187:27–48, 2016.
- [17] B. Hariharan, P. Arbeláez, R. Girshick, and J. Malik. Simultaneous detection and segmentation. In *European Conference on Computer Vision*, pages 297–312. Springer, 2014.
- [18] K. He, G. Gkioxari, P. Dollár, and R. Girshick. Mask r-cnn. In *Proceedings of the IEEE international conference on computer vision*, pages 2961–2969, 2017.
- [19] K. He, X. Zhang, S. Ren, and J. Sun. Spatial pyramid pooling in deep convolutional networks for visual recognition. *IEEE transactions on pattern analysis and machine intelligence*, 37(9):1904–1916, 2015.
- [20] K. He, X. Zhang, S. Ren, and J. Sun. Deep residual learning for image recognition. In *Proceedings of the IEEE conference on computer vision and pattern recognition*, pages 770–778, 2016.
- [21] P. Hu and D. Ramanan. Finding tiny faces. In *Proceedings of the IEEE conference on computer vision and pattern recognition*, pages 951–959, 2017.
- [22] J. Huang, V. Rathod, C. Sun, M. Zhu, A. Korattikara, A. Fathi, I. Fischer, Z. Wojna, Y. Song, S. Guadarrama, et al. Speed/accuracy trade-offs for modern convolutional object detectors. In *Proceedings of the IEEE conference on computer vision and pattern recognition*, pages 7310–7311, 2017.
- [23] A. Krizhevsky, I. Sutskever, and G. E. Hinton. Imagenet classification with deep convolutional neural networks. In *Advances in neural information processing systems*, pages 1097–1105, 2012.
- [24] J. Lee, E. Kim, S. Lee, J. Lee, and S. Yoon. Ficklenet: Weakly and semi-supervised semantic image segmentation using stochastic inference. *arXiv preprint arXiv:1902.10421*, 2019.

- [25] T.-Y. Lin, P. Dollár, R. Girshick, K. He, B. Hariharan, and S. Belongie. Feature pyramid networks for object detection. In *Proceedings of the IEEE Conference on Computer Vision and Pattern Recognition*, pages 2117–2125, 2017.
- [26] T.-Y. Lin, M. Maire, S. Belongie, J. Hays, P. Perona, D. Ramanan, P. Dollár, and C. L. Zitnick. Microsoft coco: Common objects in context. In *European conference on computer vision*, pages 740–755. Springer, 2014.
- [27] I. Loshchilov and F. Hutter. Sgdr: Stochastic gradient descent with warm restarts. *arXiv preprint arXiv:1608.03983*, 2016.
- [28] A. Newell, K. Yang, and J. Deng. Stacked hourglass networks for human pose estimation. In *European Conference on Computer Vision*, pages 483–499. Springer, 2016.
- [29] E. Ohn-Bar and M. M. Trivedi. To boost or not to boost? on the limits of boosted trees for object detection. In *2016 23rd international conference on pattern recognition (ICPR)*, pages 3350–3355. IEEE, 2016.
- [30] J. Pang, W. Sun, J. S. Ren, C. Yang, and Q. Yan. Cascade residual learning: A two-stage convolutional neural network for stereo matching. In *Proceedings of the IEEE International Conference on Computer Vision*, pages 887–895, 2017.
- [31] G. Papandreou, L.-C. Chen, K. P. Murphy, and A. L. Yuille. Weakly-and semi-supervised learning of a deep convolutional network for semantic image segmentation. In *Proceedings of the IEEE international conference on computer vision*, pages 1742–1750, 2015.
- [32] A. Paszke, S. Gross, S. Chintala, G. Chanan, E. Yang, Z. DeVito, Z. Lin, A. Desmaison, L. Antiga, and A. Lerer. Automatic differentiation in pytorch. 2017.
- [33] S. Ren, K. He, R. Girshick, and J. Sun. Faster r-cnn: Towards real-time object detection with region proposal networks. In C. Cortes, N. D. Lawrence, D. D. Lee, M. Sugiyama, and R. Garnett, editors, *Advances in Neural Information Processing Systems 28*, pages 91–99. Curran Associates, Inc., 2015.
- [34] O. Ronneberger, P. Fischer, and T. Brox. U-net: Convolutional networks for biomedical image segmentation. In *International Conference on Medical image computing and computer-assisted intervention*, pages 234–241. Springer, 2015.
- [35] O. Russakovsky, J. Deng, H. Su, J. Krause, S. Satheesh, S. Ma, Z. Huang, A. Karpathy, A. Khosla, M. Bernstein, et al. Imagenet large scale visual recognition challenge. *International journal of computer vision*, 115(3):211–252, 2015.
- [36] B. C. Russell, A. Torralba, K. P. Murphy, and W. T. Freeman. Labelme: a database and web-based tool for image annotation. *International journal of computer vision*, 77(1-3):157–173, 2008.
- [37] J. Seo, S. Chae, J. Shim, D. Kim, C. Cheong, and T.-D. Han. Fast contour-tracing algorithm based on a pixel-following method for image sensors. *Sensors*, 16(3), 2016.
- [38] K. Simonyan and A. Zisserman. Very deep convolutional networks for large-scale image recognition. *arXiv preprint arXiv:1409.1556*, 2014.
- [39] G. Song, Y. Liu, M. Jiang, Y. Wang, J. Yan, and B. Leng. Beyond trade-off: Accelerate fcn-based face detector with higher accuracy. In *Proceedings of the IEEE Conference on Computer Vision and Pattern Recognition*, pages 7756–7764, 2018.
- [40] J. Suarez, Y. Du, P. Isola, and I. Mordatch. Neural mmo: A massively multiagent game environment for training and evaluating intelligent agents. In *Proceedings of the IEEE International Conference on Computer Vision*, pages 2021–2029, 2015.
- [41] S. Suzuki et al. Topological structural analysis of digitized binary images by border following. *Computer vision, graphics, and image processing*, 30(1):32–46, 1985.
- [42] C. Szegedy, S. Ioffe, V. Vanhoucke, and A. A. Alemi. Inception-v4, inception-resnet and the impact of residual connections on learning. In *Thirty-First AAAI Conference on Artificial Intelligence*, 2017.
- [43] X. Tang, D. K. Du, Z. He, and J. Liu. Pyramidbox: A context-assisted single shot face detector. In *Proceedings of the European Conference on Computer Vision (ECCV)*, pages 797–813, 2018.
- [44] A. Vaswani, N. Shazeer, N. Parmar, J. Uszkoreit, L. Jones, A. N. Gomez, Ł. Kaiser, and I. Polosukhin. Attention is all you need. In *Advances in Neural Information Processing Systems*, pages 5998–6008, 2017.
- [45] O. Vinyals, T. Ewalds, S. Bartunov, P. Georgiev, A. S. Vezhnevets, M. Yeo, A. Makhzani, H. Küttler, J. Agapiou, J. Schrittwieser, et al. Starcraft ii: A new challenge for reinforcement learning. *arXiv preprint arXiv:1708.04782*, 2017.
- [46] J. Wang, Y. Yuan, and G. Yu. Face attention network: an effective face detector for the occluded faces. *arXiv preprint arXiv:1711.07246*, 2017.
- [47] Y. Wang, X. Ji, Z. Zhou, H. Wang, and Z. Li. Detecting faces using region-based fully convolutional networks. *arXiv preprint arXiv:1709.05256*, 2017.
- [48] J. Xie, T. He, Z. Zhang, H. Zhang, Z. Zhang, and M. Li. Bag of tricks for image classification with convolutional neural networks. *arXiv preprint arXiv:1812.01187*, 2018.
- [49] S. Yang, P. Luo, C.-C. Loy, and X. Tang. Wider face: A face detection benchmark. In *Proceedings of the IEEE conference on computer vision and pattern recognition*, pages 5525–5533, 2016.
- [50] S. Yang, Y. Xiong, C. C. Loy, and X. Tang. Face detection through scale-friendly deep convolutional networks. *arXiv preprint arXiv:1706.02863*, 2017.
- [51] K. Zhang, Z. Zhang, Z. Li, and Y. Qiao. Joint face detection and alignment using multitask cascaded convolutional networks. *IEEE Signal Processing Letters*, 23(10):1499–1503, 2016.
- [52] Z.-H. Zhou. A brief introduction to weakly supervised learning. *National Science Review*, 5(1):44–53, 08 2017.
- [53] Y. Zhu, C. Zhao, J. Wang, X. Zhao, Y. Wu, and H. Lu. Couplet: Coupling global structure with local parts for object detection. In *Proceedings of the IEEE International Conference on Computer Vision*, pages 4126–4134, 2017.
- [54] C. L. Zitnick and P. Dollár. Edge boxes: Locating object proposals from edges. In *European conference on computer vision*, pages 391–405. Springer, 2014.